

Research Article

A Study on the Separation Length of Shock Wave/Turbulent Boundary Layer Interaction

Yong-yi Zhou ¹, Yi-long Zhao ², and Yu-xin Zhao ¹

¹Science and Technology on Scramjet Laboratory, College of Aerospace Science and Engineering, National University of Defense Technology, Changsha, Hunan 410073, China

²Unmanned Systems Research Center, National Innovation Institute of Defense Technology, Academy of Military Sciences, Beijing 100071, China

Correspondence should be addressed to Yi-long Zhao; zhaoyilong@nudt.edu.cn

Received 11 June 2019; Revised 22 August 2019; Accepted 20 September 2019; Published 20 October 2019

Academic Editor: Giovanni Delibra

Copyright © 2019 Yong-yi Zhou et al. This is an open access article distributed under the Creative Commons Attribution License, which permits unrestricted use, distribution, and reproduction in any medium, provided the original work is properly cited.

The separation length of shock wave/boundary layer interaction (SWBLI) was studied by a numerical method, which was validated by experimental results. The computational domain was two-dimensional (2-D). The flow field was an incident oblique shock interacting with a turbulent boundary layer on a flat adiabatic plate. According to the simulation data, the dependency of the separation length on the relevant flow parameters, such as the incident shock strength, Reynolds number, and Mach number, was analyzed in the range of $2 \leq M \leq 7$. Based on the relations with the flow parameters, two models of the separation length at low and high Mach numbers were proposed, respectively, which can be used to predict the extent of the separation in the SWBLI.

1. Introduction

The prediction of the SWBLI is a formidable challenge for the supersonic and hypersonic aircraft engineer [1]. The SWBLI can be found in transonic/supersonic airfoil flows, the inflow and outflow of the supersonic or hypersonic cruising aircrafts, atmosphere reentry vehicles, and gas turbines. The SWBLI is an extremely complicated flow which involves the viscous-inviscid interaction and has been studied for many years. Reviews of experimental and theoretical investigations can be found in Green [2], Delery [3], and Zheltovodov [4].

The supersonic boundary layer separation is a “free interaction” process between the boundary layer and the outer supersonic flow. The flow properties in the vicinity of the separation point are independent of the downstream flow conditions. Stewartson [5], who exhibited a triple deck structure in the interaction zone, studied the SWBLI at the high Reynolds number using “asymptotic analysis.” Brown and

Williams [6] and Rizzetta et al. [7] made more researches based on the triple-deck analysis.

Figure 1 shows the schematic description of the incident shock-induced boundary layer separation. The incident shock forms sharp adverse pressure gradients in the boundary layer, which causes the separation of the boundary layer. The separation starts at the S point. The separation bubble induces a separation shock. Due to the constant pressure in the separation bubble, the incident shock reflects on the bubble and forms expansion waves. The shear layer reattaches at the R point where the separation bubble ends. The shear layer turns towards the wall which generates compression waves. The compression waves merge into reattachment shock in the mainstream. The distance from the separation point to the reattachment point is defined as the separation length, l_s .

Neiland [8] proposed that the “asymptotic structure” of the circumfluence is in the separated boundary layer. Based on this, Stewartson and Williams [9] studied the large-scale

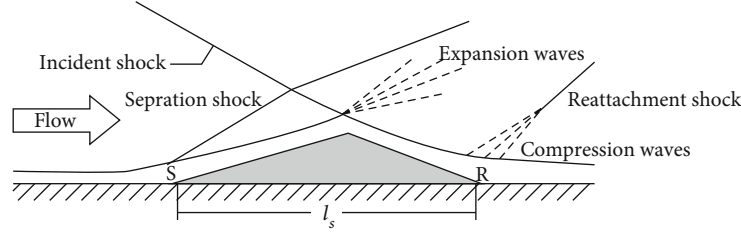


FIGURE 1: Schematic description of incident shock induced boundary layer separation.

separation of the laminar boundary layer induced by strong shock wave. Results showed that the separation length can be predicted by

$$\frac{l_s}{\delta_0^*} \frac{M_1^3}{\sqrt{\text{Re}_{x_0}/C}} = K_S(M_1) \left(\frac{p_3 - p_{\text{inc}}}{p_1} \right)^{3/2}, \quad (1)$$

where

$$K_S(M_1) = 19 \frac{(T_w/T_1)^{3/2}}{1.72 + 1.11(\gamma - 1)M_1^2}, \quad (2)$$

$$C = \frac{\mu_w}{\mu_1} \frac{T_1}{T_w}$$

is the Chapman-Rubesin constant. The model shows that the separation length increases with the $3/2^{\text{th}}$ power of the pressure gradient. However, Katzer [10] showed that the separation length increases linearly with the pressure gradient based on numerical data. The model yields

$$\frac{l_s}{\delta_0^*} \frac{M_1^3}{\sqrt{\text{Re}_{x_0}/C}} = 4.4 \frac{p_3 - p_{\text{inc}}}{p_1}. \quad (3)$$

Davis and Sturtevant [11] studied the separation length of the laminar boundary layer in high enthalpy compression corner flow. The real-gas effects were investigated as well.

Most studies on separation length were focused on the laminar separation. The turbulent separation is much more complex. Settles et al. [12] studied the turbulent separation length of compression corner flow at Mach 3. They proposed an empirical model. It was found that the separation length increases with the Reynolds number at low Reynolds number flow ($\text{Re}_\delta < 10^5$), but conversely at high Reynolds number

flow ($\text{Re}_\delta > 10^5$). Zheltovodov et al. [13] investigated the SWBLI in the 2-D compression corner flow experimentally and established the relationship between the separation length and Reynolds number.

The unsteadiness of the SWBLI has been investigated widely recently. Dolling and Murphy [14] proposed that the low-frequency oscillation of the SWBLI is the result of the internal dynamics of the separation bubble. Erengil and Dolling [15] studied the unsteadiness of the corner separation experimentally at Mach 5 and showed that the characteristic frequency range of the separation shock increases as the size of the separation bubble reduces. Dupont et al. [16], Pionniau et al. [17], and Souverein et al. [18] found that when separation occurs most of the time, the separation bubble pulsation will become predominant and involve very low frequencies. Pirozzoli and Grasso [19] proposed that the large-scale unsteadiness is associated with an acoustic feedback mechanism in the separation bubble. The above researches have shown that the unsteadiness of the SWBLI is greatly related to the size of the separation bubble.

In this paper, we analyze the separation length in 2-D incident shock-induced turbulent boundary layer separation in a wide range of Mach numbers ($2 \leq M_1 \leq 7$). The boundary layer is generated by a flat plate. The relation between the separation length and the relevant flow parameters such as the incident shock strength, Mach number, and Reynolds number is analyzed with experimental and numerical methods. Two mathematical models are proposed to predict the separation length at low and high Mach numbers.

2. Numerical Methods and Validation

2.1. Numerical Methods. The two-dimensional and compressible form of Reynolds-averaged Navier-Stokes (RANS) method has been applied to this numerical simulation. The governing equations are as follows:

$$\begin{aligned} \text{Continuity equation : } & \frac{\partial \rho}{\partial t} + \frac{\partial}{\partial x_i}(\rho u_i) = 0, \\ \text{Momentum equation : } & \frac{D(\rho u_i)}{Dt} = -\frac{\partial p}{\partial x_i} + \frac{\partial}{\partial x_j} \left[\mu_{\text{eff}} \left(\frac{\partial u_i}{\partial x_j} + \frac{\partial_j}{\partial x_i} - \frac{2}{3} \delta_{ij} \frac{\partial u_k}{\partial x_k} \right) \right] + \frac{\partial}{\partial x_j} (-\rho \overline{u_i' u_j'}), \\ \text{Energy equation : } & \frac{\partial}{\partial t}(\rho E) + \frac{\partial}{\partial x_i} [u_i(\rho E + p)] = \frac{\partial}{\partial x_i} \left[\left(\alpha + \frac{C_p \mu_t}{P_{rt}} \right) \frac{\partial T}{\partial x_i} + u_j (\tau_{ij})_{\text{eff}} \right], \end{aligned} \quad (4)$$

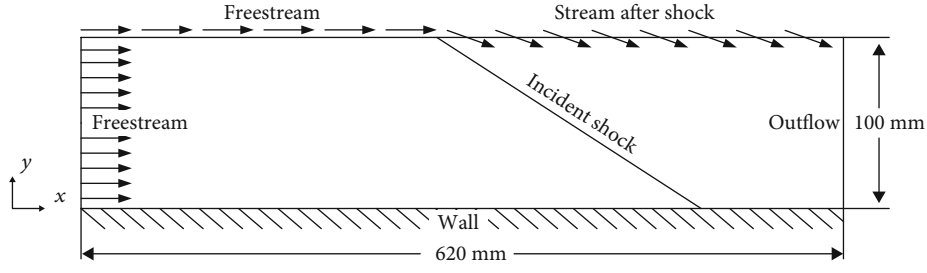


FIGURE 2: Computational domain and the boundary conditions.

where E and T are the mass-averaged values and τ_{ij} is the stress tensor and is defined as follows:

$$\tau_{ij} = \mu_{\text{eff}} \left(\frac{\partial u_j}{\partial x_i} + \frac{\partial u_i}{\partial x_j} \right) + \frac{2}{3} \mu_{\text{eff}} \frac{\partial u_i}{\partial x_i} \delta_{ij}. \quad (5)$$

The term δ_{ij} is the viscous heating caused by the dissipation. The state equation of perfect gas is applied to closure the equations.

$$p = \rho RT. \quad (6)$$

The Spalart-Allmaras turbulence model [20], which is reported suitable for the hypersonic flow simulation, was used in the present work. The second-order spatially accurate upwind scheme (SOU) and the advection upstream splitting method (AUSM) flux vector splitting were employed to accelerate convergence. The air was assumed to be a perfect gas, of which the specific heat ratio was 1.4. The viscosity of the gas was calculated according to Sutherland's law.

$$\frac{\mu}{\mu_0} = \left(\frac{T}{T_0} \right)^{1.5} \left(\frac{T_0 + T_s}{T + T_s} \right). \quad (7)$$

The computational domain and the boundary conditions are shown in Figure 2. The length in the x -direction was 620 mm, and the height in the y -direction was 100 mm, which was partitioned into a 310 (length) \times 200 (height) structured mesh. The inflow condition was set to be freestream condition. The incident shock was usually generated by a compression wedge. However, there will be expansion waves at the end of the compression wedge. In order to generate the incident shock and avoid the expansion waves at the same time, the upper boundary of the computational domain was divided into two parts (before and after the incident shock). The flow before the incident shock was set to be freestream condition, and the flow after the incident shock was specified according to the Rankine-Hugoniot relations across the shock. The outflow was extrapolated. The adiabatic and no-slip wall conditions are applied on the wall.

2.2. Validation for Grid and Boundary Layer Simulation. The influence of the grid distribution on the simulation of boundary layer is analyzed. Three cases with coarse, medium, and fine near wall grid are simulated, and the resultant velocity profiles are compared with Spalding's

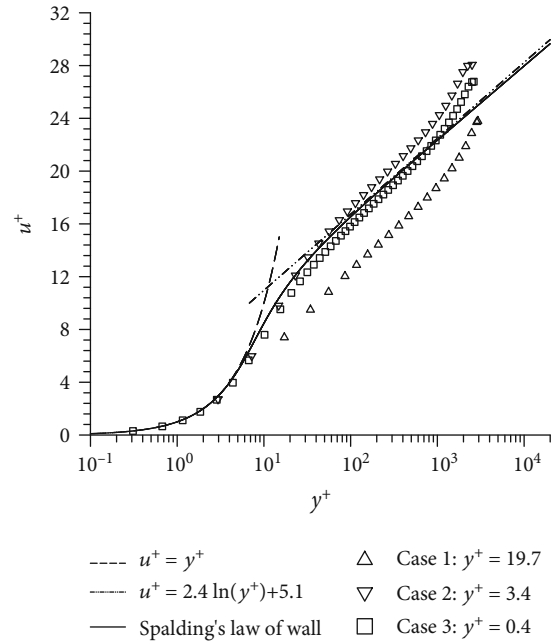


FIGURE 3: Comparison of simulated velocity profiles with Spalding's law of wall.

law of wall in Figure 3. The simulation is carried out according to the physical parameters of the wind tunnel. The Mach number of the incoming flow is 2.92. The inflow static temperature and pressure are 300 K and 1 atm, respectively. The unit Reynolds number is $\text{Re} = 8.01 \times 10^6 \text{ m}^{-1}$. The Spalart-Allmaras turbulence model is used. The wall is adiabatic and with no slip. The boundary layer velocity thickness $\delta_{0.99}$ where the profile is extracted is 8 mm. Compressible Spalding's law of the wall [21] is transformed by van Driest transformation [22]. The simulated boundary layer profile of case 3 with $y^+ = 0.4$ corresponds well with Spalding's law of wall. The near-wall grid of all the simulated cases in the paper is the same as that of case 3.

2.3. Validation for SWBLI Simulation at Low Mach Number. The numerical methods were validated by experiments. The experiments of SWBLI were conducted in an indraft supersonic wind tunnel at $M = 2.92$ [23, 24]. The size of the test section is 400 mm in length, 200 mm in width, and 200 mm in height. The unit Reynolds number is $\text{Re} = 8.01 \times 10^6 \text{ m}^{-1}$.

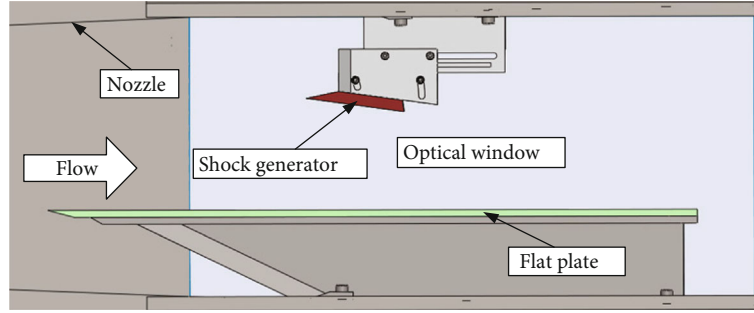


FIGURE 4: Experiment model in the wind tunnel.

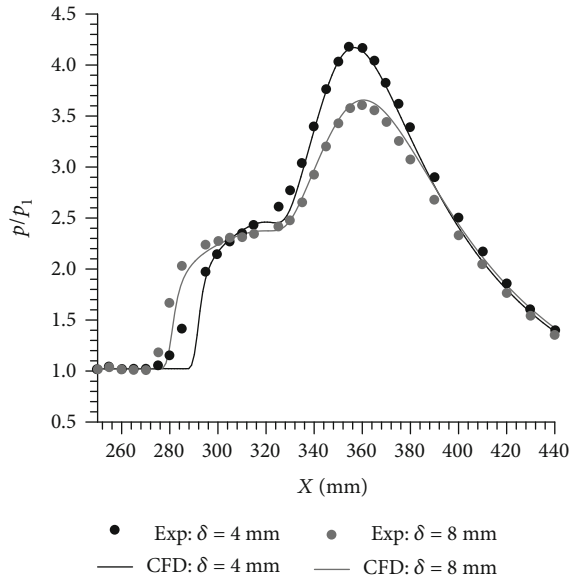


FIGURE 5: Comparison of static wall pressure of CFD and experiments.

Figure 4 shows the experiment model in the test section of the wind tunnel. A flat plate is fixed on the lower wall, which is parallel with the inflow. The compression wedge, which generates the incident oblique shock, is fixed on the upper wall of the test section. In this validation, the deflection angle is 15 deg. To generate a turbulent boundary layer with different thicknesses at the incident point, two types of the flat plates are used in this validation. The first one is shown in Figure 4. The horizontal distance from the leading edge to the shock generator of the plate is 80 mm and 430 mm of the other plate. The inviscid incident point of the oblique shock on the flat plate is 270 mm apart from the leading edge of the shock generator. The velocity thicknesses of boundary layers are 4 mm and 8 mm at the incident point, respectively. Both flat plates are in the effective zone of the nozzle. The width of the flat plate and the shock generator is 196 mm, with a 2 mm distance to the sidewalls of the test section on each side. The static pressure along the center line of the flat plate is measured with PSI-9116 pressure scanners.

Figure 5 shows the comparison of the numerical and experimental static pressure of the shock induced turbu-

lent boundary layer separation flow. The numerical simulation results agree well with the experimental data in all the test cases.

2.4. Validation for SWBLI Simulation at High Mach Number. In order to validate the numerical simulation of the SWBLI flow at the high Mach number, the experiments done by Schülein [25] are adopted as validation cases. The identical flow fields of the experiments are simulated, and the numerical results are compared with the experimental results in Figure 6. The compression angles of the shock generator of the two cases are 10 deg and 14 deg, respectively. The case with the compression angle of 10 deg corresponds to weak separation, and the other with the compression angle of 14 deg corresponds to strong separation.

Shown in Figures 6(a) and 6(b) is the static pressure and skin friction coefficient distribution of the boundary layer. The numerical pressure distribution agrees well with the experimental data in the two cases. The skin friction coefficient of the separation point and the reattachment point is regarded as 0, near which the simulation results agree well with the experimental data. However, after the reattachment point, the simulation underestimates the skin friction coefficient compared with the experimental data. The discrepancy may be attributed to the limitation of the RANS simulation of the reattachment flow [26, 27]. The discrepancy has little influence on the prediction of the separation length.

Shown in Table 1 is the comparison of the numerical and experimental separation length. Although the prediction of the skin friction coefficient is dissatisfactory for reattachment, the prediction of separation length is rather good. The discrepancy could be defined as

$$\eta = \frac{l_{S_{CFD}} - l_{S_{Exp}}}{l_{S_{Exp}}} \times 100\%. \quad (8)$$

3. Results and Analysis

According to previous studies, the separation length depends on the relevant flow parameters such as the shock strength, Mach number, and Reynolds number. In all the simulations, the adiabatic wall is assumed. The linear fitting method is used to analyze the relevancies. The

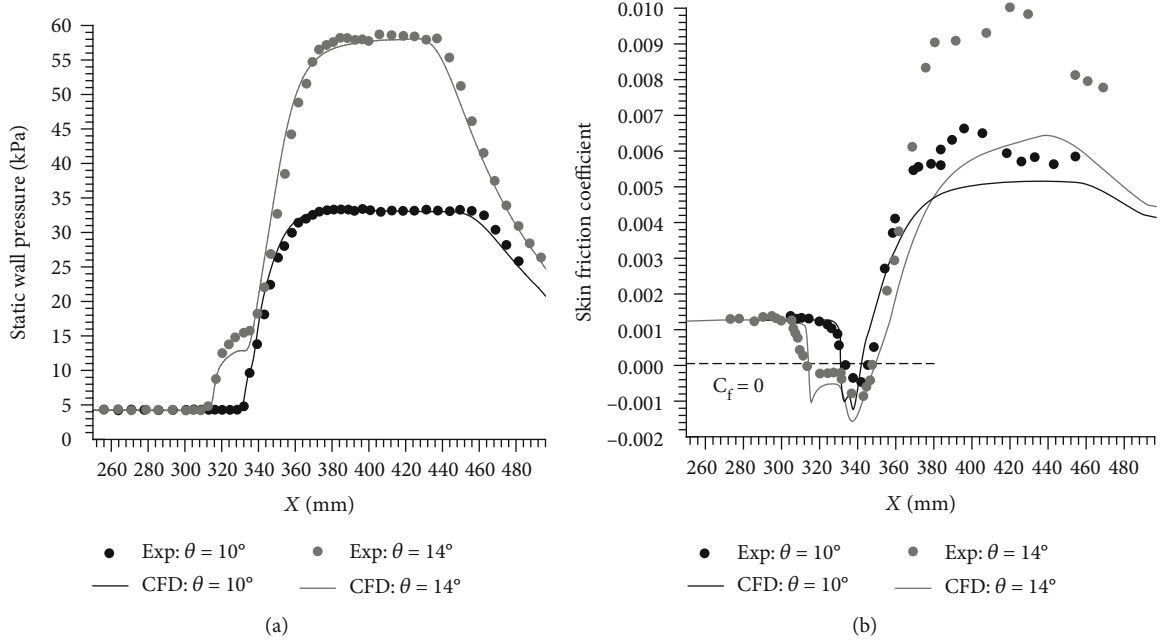


FIGURE 6: Comparison of CFD and experiments: (a) static wall pressure and (b) skin friction coefficient.

TABLE 1: Comparison of the numerical and experimental separation length.

θ	Case	x_S (mm)	x_R (mm)	l_S (mm)	Discrepancy
10 deg	Exp	333.7	344.9	11.2	-8.0%
	CFD	331.6	341.9	10.3	
14 deg	Exp	313.7	345.9	32.2	+9.9%
	CFD	314.5	349.9	35.4	

coefficient of determination R^2 , which is defined as follows, is used to evaluate the goodness of fitting:

$$R^2 = \frac{\sum_n (\hat{y}_i - \bar{y})^2}{\sum_n (y_i - \bar{y})^2}, \quad (9)$$

where \bar{y} is the average of the data and \hat{y}_i is the fitted value.

3.1. Influence of Shock Strength. Traditionally, the pressure ratio p_3/p_1 across the incident and reflected shock is usually used to measure the shock strength in the flow of shock induced separation, such as in the study of Katzer [10]. However, the pressure ratio p_3/p_1 increases greatly with the Mach number. For a wide range of Mach numbers from 2 to 7 studied herein, the separation length is more dependent on the flow deflection angle of the incident shock compared to the pressure ratio. Therefore, the flow deflection angle is used to measure the shock strength as in the study of corner separation [12, 28].

The separation length is dependent on the boundary layer and usually scaled by the local boundary layer thickness [10–13]. In the paper, the separation length l_S is scaled with the thickness of the boundary layer at the ini-

tial point of the interaction, which is denoted by δ_0 . Figure 7 shows the relationship of the flow deflection angle with the separation length. The y -axis is the $1/4^{\text{th}}$ power of the scaled separation length. The symbols of each simulated cases with different Mach numbers and Reynolds numbers located on a straight line.

It can also be seen in Figure 7 that the fitted lines intersect with the x -axis at θ_{ini} . It is defined as the initial flow deflection angle. The θ_{ini} is the flow deflection angle that corresponds to $l_S = 0$. However, l_S could not be zero because the separation occurs at much higher θ . The θ_{ini} is not a physical angle; nevertheless, it is useful for the illustration of the relationship between flow deflection angles and separation length. Based on the numerical results, the relationship between the flow deflection angle and the separation length yields

$$\frac{l_S}{\delta_0} \propto (\theta - \theta_{\text{ini}})^4. \quad (10)$$

3.2. Influence of Reynolds Number. The SWBLI is greatly influenced by the Reynolds number. Katzer [10] found that the separation length increases with the Reynolds number and proved that $l_S \propto \sqrt{\text{Re}_{x_0}}$ for a laminar boundary layer at the low Reynolds number.

The separation length is scaled with the Reynolds number. The correlation of the flow deflection angle with the separation length scaled by the Reynolds number is plotted in Figure 8. Note that the y -axis is the $1/4^{\text{th}}$ power of the scaled separation length. The figure shows that the slope of the lines is consistent at the same Mach number, which is independent of the Reynolds number. It can also be seen that the fit lines shift with the Reynolds number,

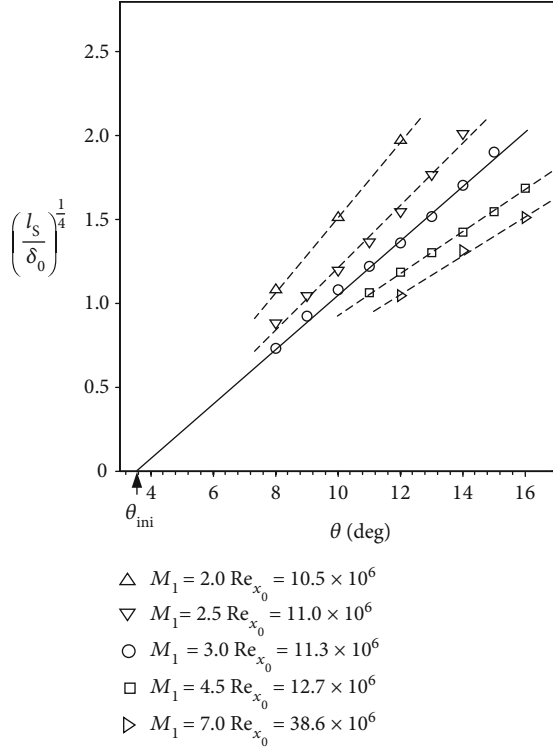


FIGURE 7: Linear fits of flow deflection angle with the separation length.

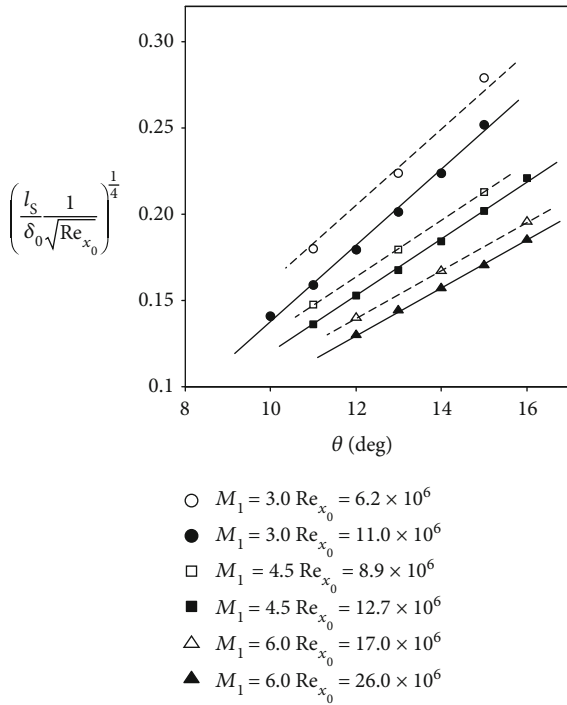


FIGURE 8: Influence of the Reynolds number on the separation length.

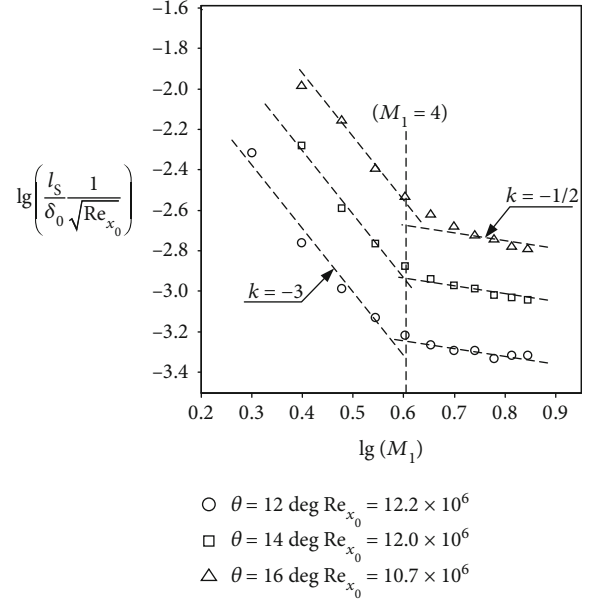


FIGURE 9: Correlation of the Mach number with the separation length.

which means that the initial flow deflection angle depends on the Reynolds number. From Figure 8,

$$\frac{l_s}{\delta_0} \frac{1}{\sqrt{\text{Re}_{x_0}}} \propto (\theta - \theta_{\text{ini}})^4. \quad (11)$$

3.3. Influence of Mach Number. The above analysis has shown that the separation length is highly dependent on the Mach number. The flow fields of shock-induced turbulent boundary layer separation from 2 to 7 are simulated. The flow deflection angles of the incident shock are 12 deg, 14 deg, and 16 deg, respectively, corresponding to weak, medium, and intensive boundary layer separations. Figure 9 shows the correlation of the Mach number with the scaled separation length. Note that the x -axis and y -axis are logarithms and \lg means logarithmic operation base 10. The figure shows that the separation length decreases with the Mach number in the whole Mach number range from 2 to 7. However, the figure also shows that the decreasing scale is different at the low Mach number and high Mach number. The inflexion occurs in the vicinity of $M_1 = 4$. So the whole range of the Mach number was divided into two parts, the low Mach number ($2 \leq M_1 \leq 4$) and the high Mach number ($4 < M_1 \leq 7$). The relations of the Mach number with the separation length were established separately.

At the low Mach number, the separation length decreases with the Mach number scaling M_1^3 , which yields

$$\frac{l_s}{\delta_0} \frac{1}{\sqrt{\text{Re}_{x_0}}} \propto \frac{1}{M_1^3}. \quad (12)$$

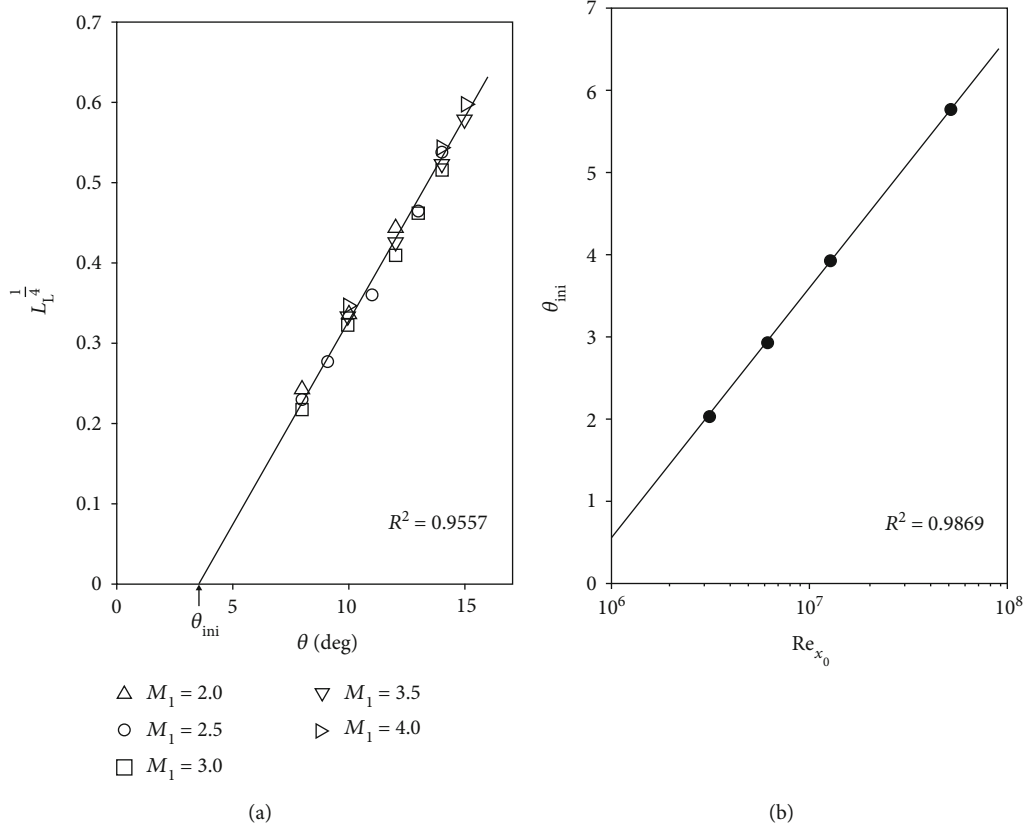


FIGURE 10: Simulated cases at the low Mach number ($2 \leq M_1 \leq 4$): (a) influence of the flow deflection angle on the separation length and (b) correlation of the Reynolds number with the initial flow deflection angle.

At the high Mach number, the separation length decreases with the Mach number scaling $M_1^{1/2}$, which yields

$$\frac{l_S}{\delta_0} \frac{1}{\sqrt{Re_{x_0}}} \propto \frac{1}{M_1^{1/2}}. \quad (13)$$

Note that the Mach number scaling at the low Mach number ($2 \leq M_1 \leq 4$) is consistent with the results of Katzer [10], which means that the relations of the Mach number with the boundary layer separation length are identical in the laminar and turbulent regimes at the low Mach number.

4. Models of the Separation Length

According to the previous analyses, the models describing the separation length can be proposed. Because the Mach number scaling is different at low and high Mach numbers, two models describing the separation length are both necessary. The similarity law of the separation length at the low Mach number ($2 \leq M_1 \leq 4$) is defined as

$$L_L = \frac{l_S}{\delta_0} \frac{M_1^3}{\sqrt{Re_{x_0}}}. \quad (14)$$

And at the high Mach number ($4 < M_1 \leq 7$),

$$L_H = \frac{l_S}{\delta_0} \frac{M_1^{1/2}}{\sqrt{Re_{x_0}}}. \quad (15)$$

4.1. Low Mach Number Model. The model of the separation length at the low Mach number is investigated first. Figure 10(a) shows the similarity law of the separation length at the low Mach number, L_L , plotted with the flow deflection angle. The Reynolds number of all the simulated cases is $Re_{x_0} = 1.2 \times 10^7$. The figure shows that, at the low Mach number, the power of the similarity law increases linearly with the flow deflection angle of the incident shock. The symbols of the different Mach numbers in the figure lie on a straight line corresponding to the same initial flow deflection angle. It means that the initial flow deflection angle is not sensitive with the Mach number. In order to simplify the model, the initial flow deflection angle is independent of the Mach number in the range of the low Mach number. Through the fitting method, the model of the separation length at the low Mach number ($2 \leq M_1 \leq 4$) is proposed as follows:

$$L_L = 72(\theta - \theta_{ini})^4. \quad (16)$$

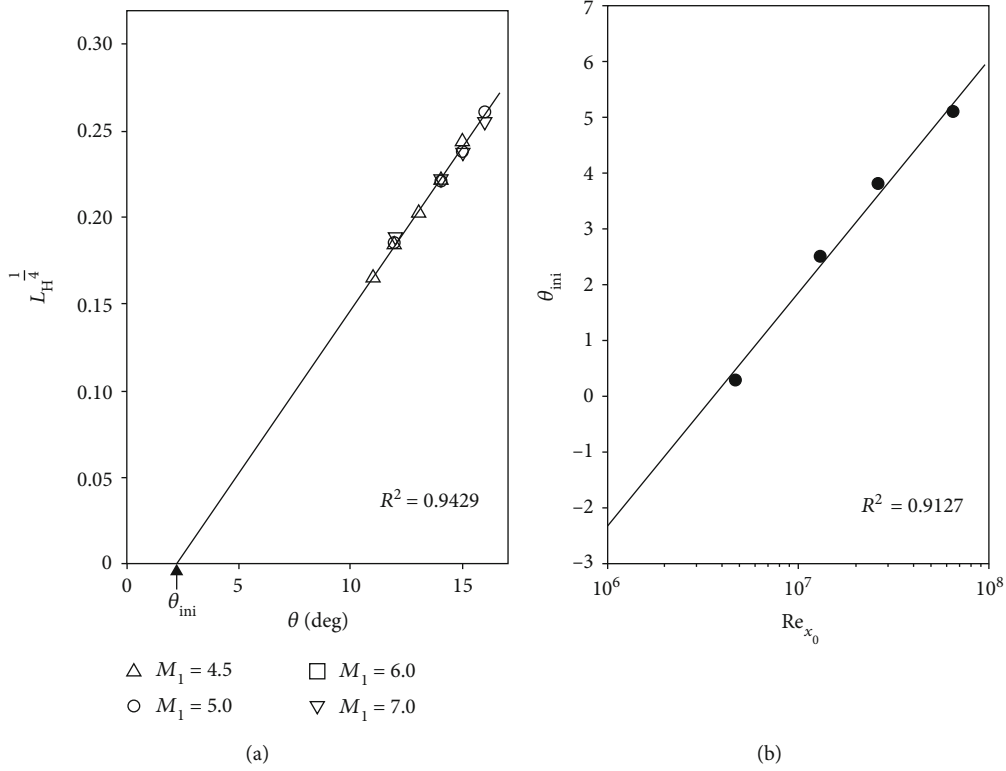


FIGURE 11: Simulated cases at the high Mach number ($4 < M_1 \leq 7$): (a) influence of the flow deflection angle on the separation length and (b) correlation of the Reynolds number with the initial flow deflection angle.

It should be noted that the unit of the flow deflection angle in the models (equation (16) to equation (19)) is radian.

The previous analysis has shown that the initial flow deflection angle depends on the Reynolds number, as seen in Figure 8. In order to investigate the correlation of the initial flow deflection angle with the Reynolds number quantitatively, the flow fields of shock-induced turbulent boundary layer separation with different Reynolds numbers at $M_1 = 3.0$ are simulated. Figure 10(b) shows the initial flow deflection angle plotted with the Reynolds number. Note that the abscissa is the logarithm of the Reynolds number. The initial flow deflection angle increases linearly with the logarithm of the Reynolds number in the studied range. Based on the numerical data, the correlation of the initial flow deflection angle with the Reynolds number at the low Mach number yields

$$\theta_{ini} = \frac{\pi}{180} [3.1 \lg(Re_{x_0}) - 18.1]. \quad (17)$$

4.2. High Mach Number Model. At the high Mach number, the boundary layers separate weakly or even do not separate if the flow deflection angle is smaller than 10 deg, so the flow deflection angles of all the simulated cases are above 10 deg. Figure 11(a) shows the similarity law of the separation length at the high Mach number, L_H , plotted with the flow deflection angle. The Reynolds number of all the cases is $Re_{x_0} = 1.2 \times 10^7$. It can be seen from the figure that the $1/4^{\text{th}}$ power of the similarity law

of separation length at the high Mach number also increases linearly with the flow deflection angle of the incident shock. The initial flow deflection angle still can be independent of the Mach number at the high Mach number. Through the fitting method, the model of the separation length at the high Mach number ($4 < M_1 \leq 7$) is proposed as follows:

$$L_H = 1.2(\theta - \theta_{ini})^4. \quad (18)$$

The influence of the Reynolds number on the initial flow deflection angle is also studied at $M_1 = 4.5$, as shown in Figure 11(b). The variation is similar to the low Mach number flows with different coefficients:

$$\theta_{ini} = \frac{\pi}{180} [4.2 \lg(Re_{x_0}) - 27.5]. \quad (19)$$

5. Conclusions

The flow of the incident shock-induced turbulent boundary layer separation on a flat adiabatic plate has been studied by experimental and numerical simulations. The compressible Reynolds-averaged Navier-Stokes equations were solved in the numerical simulation which was verified by the experiments. The study focused on the separation length of the SWBLI in a wide range of Mach numbers ($2 \leq M_1 \leq 7$).

The dependency of the separation length on the related flow parameters was analyzed. Based on the relations of the

separation length with the related flow parameters, two models describing the separation length of SWBLI at low and high Mach numbers were proposed, respectively, which can be used to predict the size of the separation bubble in the SWBLI.

In practical cases, the incident shock is usually generated by compression wedges and there are expansion waves following. It should be noted that the separation of the boundary layer will be relieved by the expansion waves, which will make the separation length shorter than the models predicted. The physical interpretation of the mechanisms of the scaling laws and analysis of the relationship of the separation size with the unsteadiness of the SWBLI are recommended as topics for a further study.

Nomenclature

M :	Mach number
M_1 :	Mach number of the freestream
x_0 :	Abscissa of the interaction start position
δ_0 :	Boundary layer thickness at x_0 (mm)
δ_0^* :	Boundary layer displacement thickness at x_0 (mm)
Re:	Reynolds number
Re_δ :	Reynolds number based on boundary layer thickness
Re_{x_0} :	Reynolds number at x_0
γ :	Specific heat ratio
p_1 :	Static pressure of the freestream (Pa)
p_2 :	Static pressure of the main stream after the incident shock (Pa)
p_3 :	Static pressure of the main stream after the reflected shock (Pa)
p_{inc} :	Shock strength for incipient boundary layer separation (Pa)
S:	Separation position
R:	Reattachment position
x_S :	Abscissa of the separation position (mm)
x_R :	Abscissa of the reattachment position (mm)
l_S :	Separation length (mm)
θ :	Flow deflection angle of the incident shock
θ_{ini} :	Initial flow deflection angle
T_1 :	Static temperature of the freestream (K)
T_w :	Wall temperature (K)
μ_1 :	Dynamic viscosity of the freestream ($N \cdot s/m^3$)
μ_w :	Dynamic viscosity at the wall ($N \cdot s/m^3$)
L_L :	Low Mach number scaling
L_H :	High Mach number scaling.

Subscripts

w :	Value at the wall
0:	Value at the interaction start
1:	Freestream value
2:	Value after the incident shock
3:	Value after the reflected shock.

Data Availability

The data used to support the findings of this study have not been made available because the disclosure of data is not permitted by the college.

Conflicts of Interest

The authors declare that there is no conflict of interest regarding the publication of this paper.

Acknowledgments

This work was supported by the National Natural Science Foundation of China (Grant No. 11502294).

References

- [1] D. J. Lusher, S. P. Jammy, and N. D. Sandham, "Shock-wave/-boundary-layer interactions in the automatic source-code generation framework OpenSBLI," *Computers & Fluids*, vol. 173, pp. 17–21, 2018.
- [2] J. E. Green, "Interactions between shock waves and turbulent boundary layers," *Progress in Aerospace Sciences*, vol. 11, pp. 235–340, 1970.
- [3] J. M. Delery, "Shock wave/turbulent boundary layer interaction and its control," *Progress in Aerospace Sciences*, vol. 22, no. 4, pp. 209–280, 1985.
- [4] A. Zheltovodov, "Some advances in research of shock wave turbulent boundary layer interactions," in *44th AIAA Aerospace Sciences Meeting and Exhibit*, pp. 1–25, Reno, Nevada, January 2006.
- [5] K. Stewartson, "Multistructured boundary layers on flat plates and related bodies," *Advances in Applied Mechanics*, vol. 14, pp. 145–239, 1974.
- [6] S. N. Brown and P. G. Williams, "Self-induced separation. III," *IMA Journal of Applied Mathematics*, vol. 16, no. 2, pp. 175–191, 1975.
- [7] D. P. Rizzetta, O. R. Burggraf, and R. Jenson, "Triple-deck solutions for viscous supersonic and hypersonic flow past corners," *Journal of Fluid Mechanics*, vol. 89, no. 3, p. 535, 1978.
- [8] V. Y. Neiland, "Flow behind the boundary layer separation point in a supersonic stream," *Fluid Dynamics*, vol. 6, no. 3, pp. 378–384, 1973.
- [9] K. Stewartson and P. G. Williams, "On self-induced separation II," *Mathematika*, vol. 20, no. 1, pp. 98–108, 1973.
- [10] E. Katzer, "On the lengthscales of laminar shock/boundary-layer interaction," *Journal of Fluid Mechanics*, vol. 206, p. 477, 1989.
- [11] J. P. Davis and B. Sturtevant, "Separation length in high-enthalpy shock/boundary-layer interaction," *Physics of Fluids*, vol. 12, no. 10, pp. 2661–2687, 2000.
- [12] G. Settles, J. Perkins, and S. Bogdonoff, "Upstream influence scaling of 2D and 3D shock/turbulent boundary layer interactions at compression corners," in *19th Aerospace Sciences Meeting*, St. Louis, MO, USA, January 1981.
- [13] A. A. Zheltovodov, É. K. Shilein, and C. C. Horstman, "Development of separation in the region where a shock interacts with a turbulent boundary layer perturbed by rarefaction waves," *Journal of Applied Mechanics and Technical Physics*, vol. 34, no. 3, pp. 346–354, 1993.
- [14] D. S. Dolling and M. T. Murphy, "Unsteadiness of the separation shock wave structure in a supersonic compression ramp flowfield," *AIAA Journal*, vol. 21, no. 12, pp. 1628–1634, 1983.
- [15] M. E. Erengil and D. S. Dolling, "Effects of sweepback on unsteady separation in Mach 5 compression ramp interactions," *AIAA Journal*, vol. 31, no. 2, pp. 302–311, 1993.

- [16] P. Dupont, C. Haddad, and J. F. Debiève, "Space and time organization in a shock-induced separated boundary layer," *Journal of Fluid Mechanics*, vol. 559, p. 255, 2006.
- [17] S. Piponniau, J. P. Dussauge, J. F. Debiève, and P. Dupont, "A simple model for low-frequency unsteadiness in shock-induced separation," *Journal of Fluid Mechanics*, vol. 629, pp. 87–108, 2009.
- [18] L. J. Souverein, P. Dupont, J.-F. Debiève, B. W. van Oudheusden, and F. Scarano, "Effect of interaction strength on unsteadiness in shock-wave-induced separations," *AIAA Journal*, vol. 48, no. 7, pp. 1480–1493, 2010.
- [19] S. Pirozzoli and F. Grasso, "Direct numerical simulation of impinging shock wave/turbulent boundary layer interaction at $M = 2.25$," *Physics of Fluids*, vol. 18, no. 6, article 065113, 2006.
- [20] P. Spalart and S. Allmaras, "A one-equation turbulence model for aerodynamic flows," in *30th Aerospace Sciences Meeting and Exhibit*, vol. 23, Reston, Virginia, USA, January 1992.
- [21] D. B. Spalding, "A single formula for the "law of the wall"," *Journal of Applied Mechanics*, vol. 28, no. 3, pp. 455–458, 1961.
- [22] E. R. van Driest, "Turbulent boundary layer in compressible fluids," *Journal of Spacecraft and Rockets*, vol. 40, no. 6, pp. 1012–1028, 2003.
- [23] Y. Zhao, S. Yi, L. Tian, and Z. Cheng, "Supersonic flow imaging via nanoparticles," *Science in China Series E: Technological Sciences*, vol. 52, no. 12, pp. 3640–3648, 2009.
- [24] Q. C. Wang, Z. G. Wang, and Y. X. Zhao, "The impact of streamwise convex curvature on the supersonic turbulent boundary layer," *Physics of Fluids*, vol. 29, no. 11, article 116106, 2017.
- [25] E. Schülein, "Skin friction and heat flux measurements in shock/boundary layer interaction flows," *AIAA Journal*, vol. 44, no. 8, pp. 1732–1741, 2006.
- [26] X. Xiao, J. R. Edwards, H. A. Hassan, and R. L. Gafnney, "Role of turbulent Prandtl numbers on heat flux at hypersonic Mach numbers," *AIAA Journal*, vol. 45, no. 4, pp. 806–813, 2007.
- [27] D. S. Dolling, "High-speed turbulent separated flows - consistency of mathematical models and flow physics," *AIAA Journal*, vol. 36, no. 5, pp. 725–732, 1998.
- [28] W. L. Hankey, "Prediction of incipient separation in shock-boundary-layer interactions," *AIAA Journal*, vol. 5, no. 2, pp. 355–356, 1967.

